Porous Gig-Lox TiO$_2$ Doped with N$_2$ at Room Temperature for P-Type Response to Ethanol

Emanuele Smecca [1], Salvatore Sanzaro [1], Clelia Galati [2], Lucio Renna [2], Leonardo Gervasi [2], Antonello Santangelo [2], Guglielmo Guido Condorelli [3], David Grosso [4], Thomas Bottein [4], Giovanni Mannino [1], Antonino La Magna [1] and Alessandra Alberti [1,*]

[1] National Research Council-Institute for Microelectronics and Microsystems (CNR-IMM),
  Zona Industriale—Strada VIII n°5, 95121 Catania, Italy; emanuele.smecca@imm.cnr.it (E.S.);
  salvatore.sanzaro@imm.cnr.it (S.S.); giovanni.mannino@imm.cnr.it (G.M.);
  antonino.lamagna@imm.cnr.it (A.L.M.)
[2] STMicroelectronics, Stradale Primosole 50, 95121 Catania, Italy; leonardo.gervasi@st.com (C.G.);
  lucio.renna@st.com (L.R.); leonardo.gervasi@st.com (L.G.); antonello.santangelo@st.com (A.S.)
[3] Dipartimento di Scienze Chimiche, Università degli Studi di Catania and INSTM UdR Catania,
  Viale Andrea Doria 6, 95125 Catania, Italy; guido.condorelli@unict.it
[4] Institut Matériaux Microélectronique Nanosciences de Provence (IM2NP) Aix-Marseille Université,
  13397 Marseille CEDEX 20, France; david.grosso@univ-amu.fr (D.G.); thomas.bottein@im2np.fr (T.B.)
* Correspondence: alessandra.alberti@imm.cnr.it

Abstract: Nanostructured materials represent a breakthrough in many fields of application. Above all for sensing, the use of nanostructures with a high surface/volume ratio is strategic to raise the sensitivity towards dangerous environmental gas species. A new Dc-Reactive sputtering Deposition method has been applied to grow highly porous p-type nitrogen-doped titanium oxide layers by modifying the previously developed reactive sputtering method called gig-lox. The doping of the films was achieved at room temperature by progressive incorporation of nitrogen species during the deposition process. Two different amounts of N$_2$ were introduced into the deposition chamber at flow rates of 2 and 5 standard cubic centimeter per minutes (sccm) for doping. It has been found that the N$_2$ uptake reduces the deposition rate of the TiO$_2$ film whilst the porosity and the roughness of the grown layer are not penalized. Despite the low amount of N$_2$, using 2 sccm of gas resulted in proper doping of the TiO$_2$ film as revealed by XPS Analyses. In this case, nitrogen atoms are mainly arranged in substitutional positions with respect to the oxygen atoms inside the lattice, and this defines the p-type character of the growing layer. Above this strategic structural modification, the multibranched spongy porosity, peculiar of the gig-lox growth, is still maintained. As proof of concept of the achievements, a sensing device was prepared by combining this modified gig-lox deposition method with state-of-the-art hot-plate technology to monitor the electrical response to ethanol gas species. The sensor exhibited a sensitivity of a factor of ≈2 to 44 ppm of ethanol at ≈200 °C as measured by a rise in the layer resistivity according to the p-type character of the material. At the higher temperature of ≈350 °C, the sensor turned to n-type as without doping. This behavior was related to a loss of nitrogen content inside the film during the annealing. It was indeed proved that p-type doping of a gig-lox sponge during growth is feasible, even at room temperature, without losing the layer porosity and the capability to host and detect environmental species. Moreover, the material integration on a device is simply done as the last production step. Easy TiO$_2$ doping procedures, combined with porosity, are of general purpose and interest for several applications even on flexible substrates.

Keywords: gas sensor; titanium oxide; doping; nitrogen

1. Introduction

Environmental pollution has been one of the hottest topics for the worldwide research community for long years. The presence of VOCs (volatile organic compounds), sulfur-based gases, and nitrogen dioxide in the air is one of the greatest concerns for common people. Therefore, the importance of producing good sensors for these pollutant gases is crucial for safety. To reduce material consumption and waste, these film technologies, likely solvent-free, are needed.

Titanium dioxide is one of the most-used materials in this field for the fabrication of photocatalyst devices and gas sensors [1–3]. The doping of pure TiO_2 films with nitrogen atoms is one of the most-used methods to further improve the sensitivity of TiO_2 to the environment thanks to the reduced band gap and a higher achievable conductivity [4]. The kind of doping of TiO_2 by nitrogen is a debated concern. As a matter of fact, the location of nitrogen species strongly depends on the doping procedure and conditions (e.g., oxygen reach vs. oxygen-poor ambient) [5]. Shen et al. have found that nitrogen atoms are placed mainly in an interstitial position by doping the TiO_2 through low-energy ion implantation [6]. Peng et al. have found both interstitial and substitutional nitrogen doping by microwave synthesis [7]. As a limiting drawback, engineering proper nitrogen incorporation would require processes at relatively high temperatures that are often not compatible with low-cost substrates.

In this framework, what is clear is that competition is established between nitrogen substituting oxygen in the octahedral coordination with titanium atoms and oxygen vacancies since they are mutually correlated. Once integrated into the anatase lattice, nitrogen atoms are solely coordinated to titanium atoms in an arrangement which resembles (but does not coincide with) the nitride one. It is also largely assessed that substitutional nitrogen introduces levels into the anatase bandgap, close to the top of the valence band [8,9]. Nitrogen can also arrange in interstitial positions, changing its neighborhood respect to a substitutional position, thus creating a π state 0.74 eV above the valence band [10].

Doped and porous TiO_2 layers grown by physical deposition would allow low contamination levels into the material and material reproducibility with consequent high production throughput. As the main issue, in situ doping during material growth is difficult to achieve at room temperature. Doping combined with porosity would allow for the raising of surface availability for high reactivity to environmental species. In this framework, we developed a new reactive sputtering method called gig-lox [11,12] to grow porous oxides for up-scalable, and therefore industrially compatible, solutions to be applied in high-throughput devices. The novelty of the produced material resides in its spongy fine-branched structure, homogeneously grown in a bottom-up process ($\leq$1000 nm) [11,13]. The layered architecture consists of grains separated by mesopores, with an internal structure of branched nanorods embedded in a network of pores. The material is grown at room temperature without the need of any firing process.

In this paper, we exploit a modified gig-lox methodology to grow nitrogen-doped TiO_2 porous scaffolds for gas sensing by introducing N_2 species at room temperature during the deposition process. Nitrogen incorporation was investigated in detail by several techniques to optimize the atomic arrangement. As a proof-of-concept, thin layers were purposely integrated into resistive devices equipped with micro-hot-plates for local heating with low power consumption. The high surface-to-volume ratio, the high surface reactivity, the pervasive network of voids, and the interconnected TiO_2 nano-branches offered by the spongy gig-lox TiO_2 layer allowed for getting a good sensitivity to ethanol at a low temperature.

2. Materials and Methods

Depositions of nitrogen-doped TiO_2 layers were performed using a customized Magnetron DC-pulsed Sputtering equipment fabricated by Kenosistec s.r.l. [13]. The Ar flow-rate was settled at 69 sccm (standard cm^3 per minutes) in all deposition processes. The reference deposition of undoped TiO_2 was done at room temperature, using a power of 140 W, a current of 475 mA and a voltage of

295 V (power loading 6.9 W/cm^2). For doping, 2 sccm or 5 sccm of N_2 were added to oxygen through the same inlet. Glass slices were used as substrates.

Spectroscopic Ellipsometry (SE) analyses were performed using a J.A.Woollam WASE instrument. A vertical configuration was used for the sample that was better suited to transparent samples in order to measure ellipsometric and transmittance data on the same point. Environmental ellipsometric porosimetry measurements were done using a visible (from 370 to 1000 nm) variable-angle spectroscopic ellipsometer (ESM 300 Woollam) with an atmospheric control chamber. Isopropanol (Sigma Aldrich, St. Louis, MO, USA) was chosen as the adsorbing gas. The volume of adsorbed isopropanol was followed through time-resolved measurement of the refractive index variation upon the relative pressure of the adsorbate (P/P_0) using the Cauchy models and the Bruggeman Effective Medium Approximation (J A. Woollam CompleteEASE software). The pore size distribution was then plotted using Kelvin's equation and using a model of cylindrical pores. A PHI ESCA/SAM 5600 Multi equipped with a standard Mg X-ray source was used to perform the XPS analyses. The Binding Energy scale was then calibrated by centering the adventitious/hydrocarbon carbon C 1s at 285.0 eV.

The layer morphology was evaluated by Field Emission-Scanning Electron Microscopy (FE-SEM) in cross-sectional configurations. X-ray diffraction (XRD) analyses were performed by using a D8-Discover Bruker AXS diffractometer, equipped with a Cu Kα source, in symmetric (source and detector move by the same incremental angle) and grazing incidence configuration.

A microheater plate device (MHP) based on a 1.5 μm thin suspended dielectric membrane was obtained through persistent plasma etch of bulk silicon. Over the membrane, a Pt metal layer was shaped to allow heating over 500 °C with a low voltage applied (<2 V). Onto the heater, Pt interdigitated electrodes were tailored to collect charges also from highly resistive sensing layers. Details regarding the micro-hot-plate are provided in a previous paper [12] where we describe each process step in a comprehensive flowchart. The gas sensors were tested in a chamber filled with ethanol vapors in dry conditions. The N-doped TiO_2 films were integrated into the sensors over the Pt interdigitated electrodes, as the last step process, using a shadow mask.

3. Results and Discussion

Doping of TiO_2 layers was performed by modifying the already developed gig-lox method with the additional injection of nitrogen molecules inside the deposition chamber during growth. The growth process was done at room temperature, and this represents the prerequisite of compatibility with the use of flexible substrates.

The active role of nitrogen during growth is primarily testified by the values of deposition rate shown in Table 1—the higher the content of nitrogen gas, the lower the deposition rate. This finding is likely a consequence of competition between oxidation and nitridation of the Ti species, combined with additional N–O interactions/reactions into the plasma region. This competition is expected to have effects on the nanostructure of the deposited layers. To be comparable, all the grown layers were 420nm-thick.

Table 1. Deposition rate at different contents of nitrogen gas during the process.

| Nitrogen Flux (sccm)	Deposition Rate (nm/min)
0	4.2
2	2.7
5	1.5

All the starting materials were mostly amorphous. For investigation purposes and to compare the different materials, an internal lattice structuration was triggered by annealing the samples in a furnace at 500 °C. All the lattice structures consequently settled in the anatase arrangement [14] as depicted by the diffraction patterns of Figure 1a. No other polymorphisms were present in the layers. Although the structures look similar, a difference was identified in the texturing degree of the

grains [15], a parameter that weighs the reciprocal abundance of the growing planes selected during growth. The related figures of merit are in Figure 1b wherein the relative intensities of the two main planes, namely the (101) vs. (004), were measured in the different growing conditions. Here, we note the first discontinuity when using 2 sccm of N_2 during growth—this is the only process that produced a randomly oriented set of anatase grains.
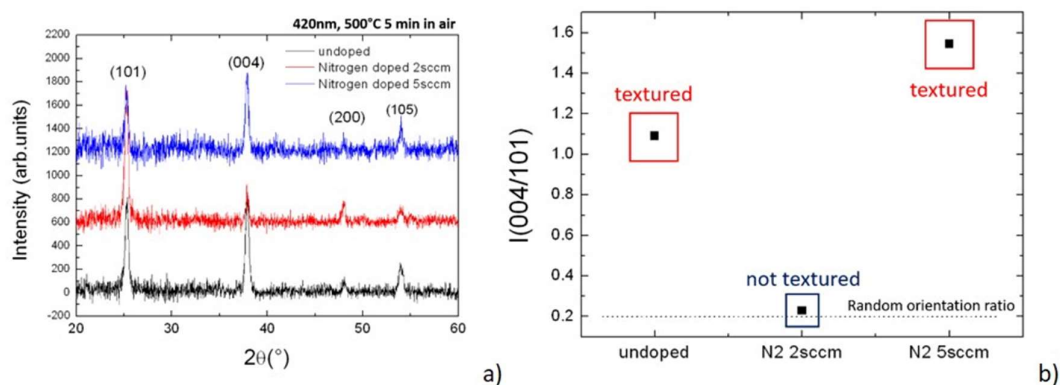

Figure 1. (**a**) X-ray diffraction pattern and (**b**) texturing parameters collected in the layers grown under the different conditions.

Grains size can be evaluated by applying the Debye–Scherrer calculation to the full width at half maximum (FWHM) of the diffraction peaks. The horizontal and vertical dimension of the nanograins can be also discriminated using different Bragg peaks acquired in symmetric and grazing geometries. The average nanodomain shape and sizes are represented in Figure 2, right panel. In the left panel, we have chosen to represent the average domain volume for two different families of grains having the [101] and [001] growth directions perpendicular to the sample surface. Here, we found a second discontinuity in the volume of the nanograins that was larger in the layer grown using 2 sccm of N_2.
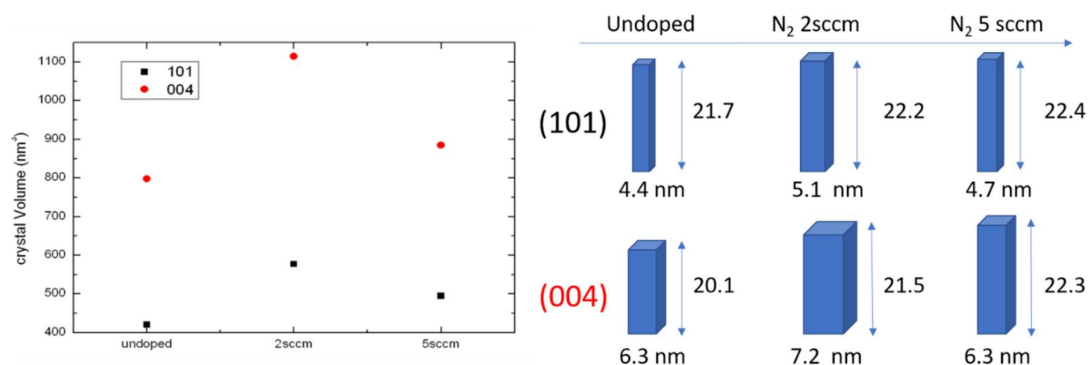

Figure 2. Nanodomain size and volume in the layers grown under the different conditions.

Figure 3 represents the described scenario by a representative SEM cross-sectional view of the material. An SEM image was taken in the as-deposited layer and, therefore, the nanostructuration was already a property of the material after deposition. According to this, and on the basis of our previous results [11–13], we argue that annealing has the main role in promoting the atomic ordering inside the nanograins without inducing drastic modification of the nano/meso structuration of the layer.
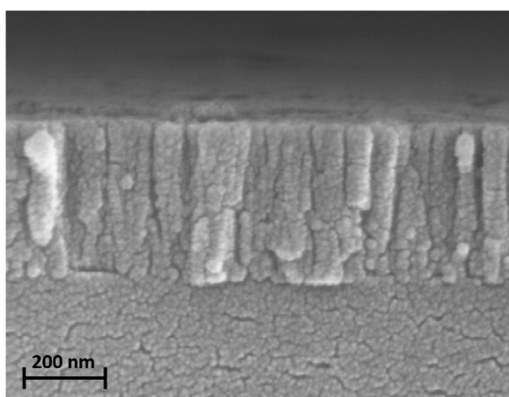
**Figure 3.** Cross-sectional SEM images of the as-deposited TiO$_2$ film.

Roughness and porosity were evaluated by spectroscopic ellipsometry. They were slightly modified by the annealing, as shown in Figure 4. The roughness of the layers decreased in all cases as well as the porosity that has been calculated using the formula in the inset of the same figure. This agrees with the behavior of undoped gig-lox layers, previously explored up to a thickness of 1000 nm [13]. As a further fingerprint of the deposition at 2 sccm of N$_2$, we found a minimum value in the porosity curve after annealing. This could likely be linked to the morphology of the grains and their size. Intermediate cases are expected by annealing at temperatures <500 °C, as occurs when applying the material in a gas-sensing device [13].
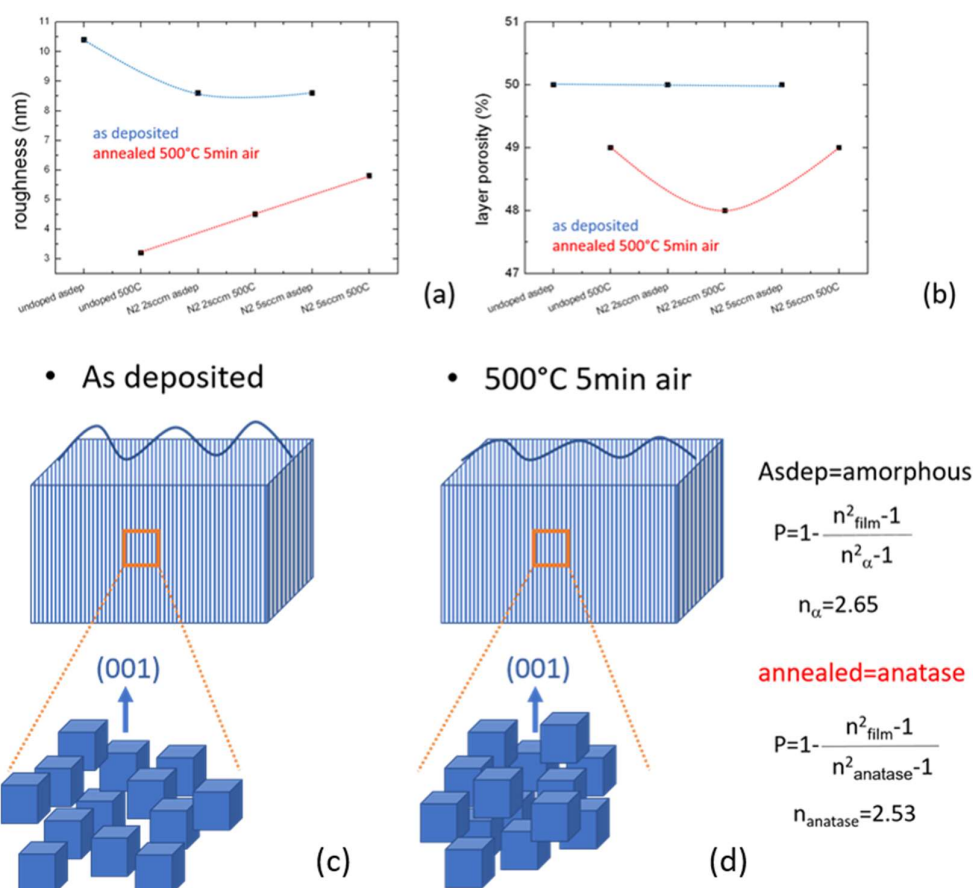
Figure 4. Roughness (**a**) and porosity (**b**) of the layers and their change after annealing at 500 °C. Schematic representation of the grain size and distribution inside the layer deposited, before (**c**) and after (**d**) annealing at 500 °C.

Environmental ellipsometry porosimetry was performed to estimate the pore dimension of the layers before and after the annealing. This parameter is crucial for the gas-sensing properties of the devices. The results of the analyses are shown in Figure 5. The size distribution of the pores shows a main peak at around 4 nm for all the as-deposited layers. After the annealing, a slight broadening of the main peak and a better definition of a second band around 10 nm was recorded. All kinds of layers indeed exhibited a bimodality in the pore size distribution, as observed in our previous publication [11]. This demonstrates that growing under nitrogen still allows for keeping the advantages of a double-size porosity. The annealing at 500 °C rearranged the structure in such a way that the nanopores' size slightly spread out, framed in a better-defined mesopore array.

Non-ambient spectroscopic ellipsometry was used to explore the dielectric constant of the materials (Figure 5a). According to what was observed in the structural findings, the annealing makes steeper e2 and shrinks e1 in all cases (the imaginary and real part of the dielectric constants, respectively). Main significant differences are highlighted by Tauc's plot in Figure 5b as follows: (a) Annealing the layer increased the bandgap in each kind of sample (including the one grown at 5 sccm not reported for simplicity); (b) the bandgap value was lowered by using N_2 during growth (e.g., from 3.44 eV to 3.57 eV in the 2s ccm N_2-grown sample); (c) differently from all the other samples, the TiO_2 layer grown under 2 sccm of nitrogen showed a long pre-gap tail, that is likely attributed to defects states into the gap [8] introduced by the nitrogen doping.
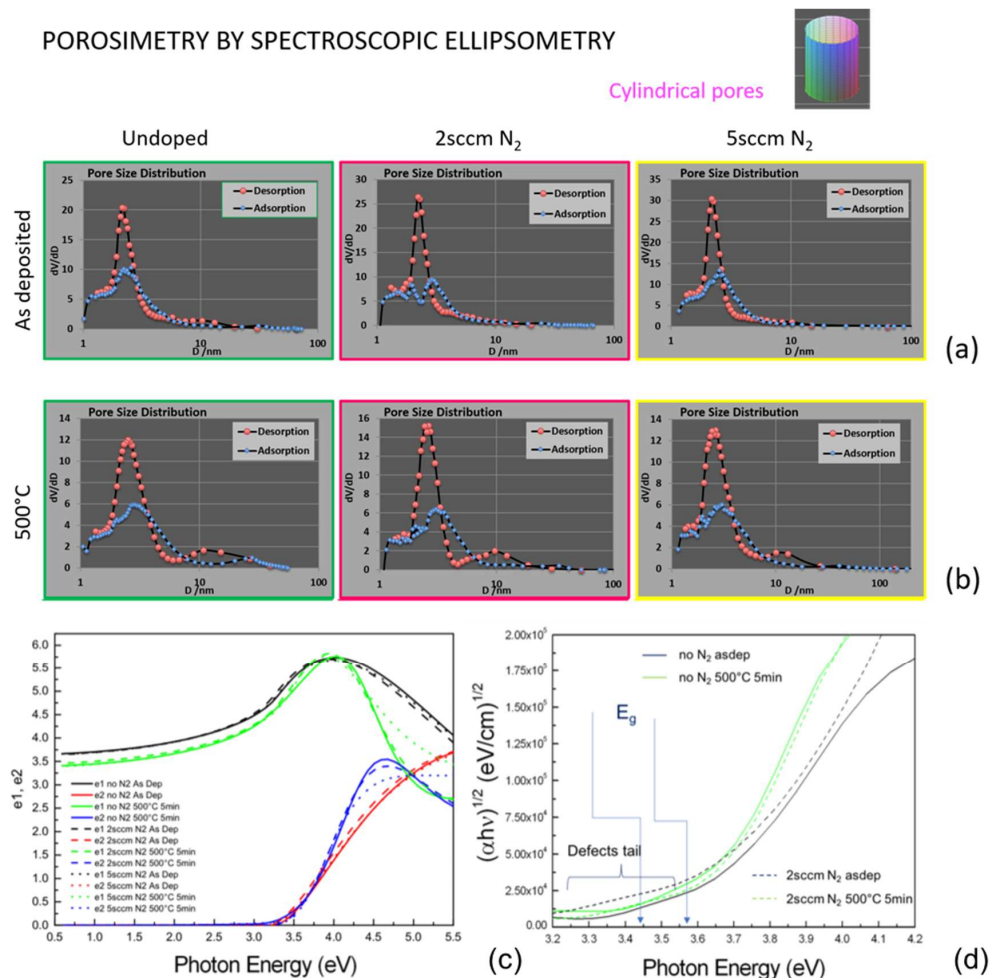
Figure 5. Environmental porosimetry analyses performed on the samples deposited at different nitrogen flux for as deposited (**a**) and annealed at 500°C (**b**) films. Lower panel: (**c**) real and imaginary parts of the dielectric constant before and after annealing in the three cases; (**d**) Tauc's plot of the absorption coefficient.

　　　XPS analyses were indeed performed to investigate the incorporation of nitrogen atoms into the TiO_2 matrix with details on the chemical surrounding and the configurational changes that occurred during annealing. Figure 6 show the existence of the N1s band for all the samples analyzed. Results on the chemical analyses are summarized in Table 2.

Table 2. Chemical composition obtained by XPS analyses performed on TiO_2 film deposited at different N_2 flux and annealed at different temperatures.

SAMPLE	N_2 (SCCM)	ANNEALING TEMPERATURE (°C)	ANN. TIME (MIN)	TI (%)	O (%)	N (%)	C (%)
1	2	no	-	15.7	50.4	2.4	31.5
2	2	200	120	10.7	34.6	1.5	53.2
3	2	500	5	17.1	54.3	1.3	27.3
4	5	no	-	16.9	53.2	1.0	28.9
5	5	200	120	10.2	35.3	0.8	53.6
6	5	500	5	17.7	54.7	0.7	26.9

　　　The large band around 400 eV in the as-deposited samples (Figure 6) resulted from two different peaks—the first one centered at 399.7 eV is the peak related to nitrogen atoms in a TiO_2 matrix that could be related to nitrogen bonded with both titanium and oxygen atoms [16], and the second one centered at $\approx$401 eV is related to nitrogen atoms in the organic form. The sample with the highest nitrogen content was the sample prepared with 2 sccm of N_2 with respect to the sample prepared at 5 sccm of N_2, despite the higher N_2 flow used during the deposition process. This result can be explained by competition established between Ti oxidation at the growing front and N_2–O_2 interaction inside the plasma region due to the particular geometry of the deposition chamber. The common inlet for the O_2 and N_2 gases is, in fact, located in the bottom part of the chamber, in close proximity to the substrate. At the lower N_2 intake, the reactive species are mostly confined above the substrate where they preferentially react with the titanium adatoms landing from the target. At higher fluxes, nitrogen species are evenly distributed inside the plasma, having an enhanced tendency to interact with oxygen into the plasma region. This likely promoted the formation of NO_x species and consequent reduction of the amount of nitrogen incorporated inside the film. Accordingly, the growth rate of the titanium oxide film reduces proportionally with increasing the flow rate of N_2 [13].

　　　As the main finding, the as-deposited samples (Figure 6) showed a peak centered at 396.7 eV due to nitrogen atoms with nitride coordination [17–19]. The presence of this peak testifies that nitrogen atoms introduced by the modified gig-lox process are positioned in the substitutional position in the crystal lattice. In this configuration, titanium atoms are positioned likely as in the TiN crystal lattice. The slight difference in the peak position with respect to the pure TiN films could be explained by the oxygen atoms as the second nearest atoms in the N–Ti–O [17,18] that are not present in the pure TiN material. The presence of the nitrogen atoms in substitutional position is also in agreement with the lower band gap ($\approx$0.13 eV) and the long pre-gap tail found in the doped layers with respect to the pure TiO_2 films. The chemical analyses obtained from the high resolution spectra are reassumed on Table 3.

Table 3. Chemical analyses and atomic % obtained by high-resolution XPS analyses.

SAMPLE	$N_{(INTERSTITIAL+CONTAMINATS)}$	$N_{SUBSTITUTIONAL}$	$O_{(OXIDE)}$	TI/O	%DOPING
1	1.31	1.09	34.14	0.46	2.15
2	1.00	0.50	31.81	0.34	1.16
3	1.30	-	43.04	0.40	0.00
4	0.78	0.22	41.71	0.41	0.38
5	0.65	0.15	20.68	0.49	0.49
6	0.70	-	40.01	0.44	0.00

　　　We have additionally performed XPS analyses on annealed samples. After annealing at 500 °C, the nitrogen content decreased, and the peak related to the nitride fully disappeared in both samples (2 sccm and 5 sccm). We, instead, found a band centered at $\approx$404 eV due to nitrite form. During

annealing, oxidation of the nitrogen atoms took place inside the film, with its partial desorption from the surface [20]. The atomic percentage of nitrogen related to the peaks at ≈400 eV and ≈401 eV was the same after the annealing process. We speculate that the annealing process oxidizes the nitrogen atoms, initially coordinated inside the film as nitrides, due to their proximity with oxygen atoms. On the other hand, the nitrogen atoms in the organic form, which are adsorbed on the surface, are not affected by the oxidation during annealing.

A different scenario was found on samples annealed at 200 °C. This temperature was chosen since it is close to typical working temperatures for sensing (a proof of concept will be given hereafter). After annealing at 200 °C, substitutional nitrogen species, although in an amount slightly decreased, still persisted as the dopant in the sample deposited at 2 sccm of N_2 (peak at 396.7 eV).
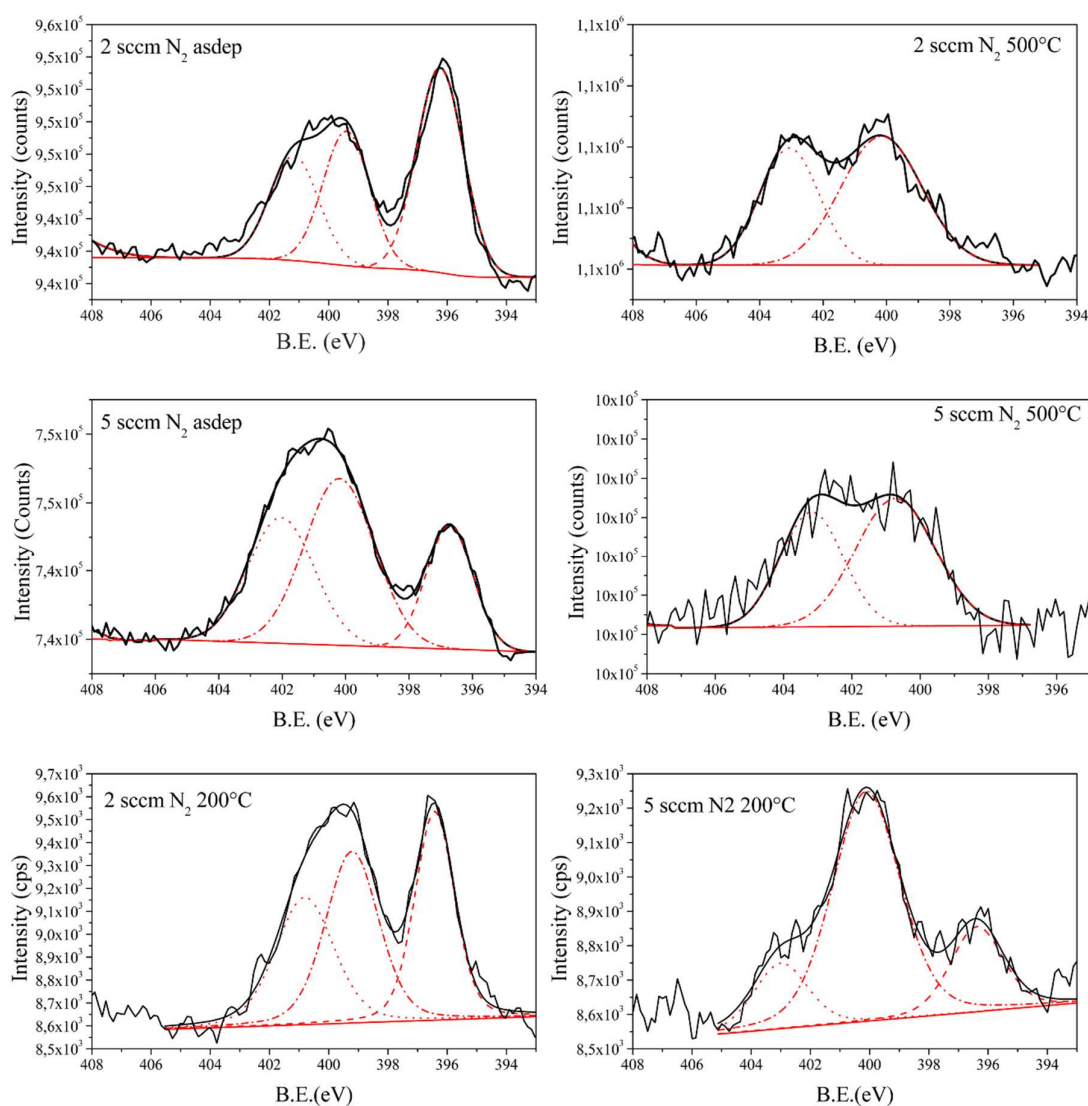

Figure 6. XPS N1s region for all the analyzed samples.

4. Application for Ethanol Sensing

As proof of concept, the layer grown at 2 sccm of nitrogen was indeed integrated into a state-of-the-art micro-hot-plate technology (Figure 7) as done in Reference [13]. The material integration was easily done as the last production step without requiring lithographic or etching processes. The gig-lox doped layer was directly deposited on the exposed area of the micro-hot-plate at room temperature, and this allowed for the preservation of all the pre-existing materials into the

device. The sensor showed a better response than the one based on the oxide grown using 5 sccm of N_2 due to the higher nitrogen doping [21,22]. The results are shown in Figure 8, in which the p-type responses, for the doped sample at two different temperatures (190 °C and 230 °C), are shown when 44 ppm of ethanol was made to flow through the reaction chamber, in dry condition. The R_{air} is the resistance measured when only air is in the chamber, while R_{gas} is the resistance measured when ethanol gas is introduced inside the chamber."

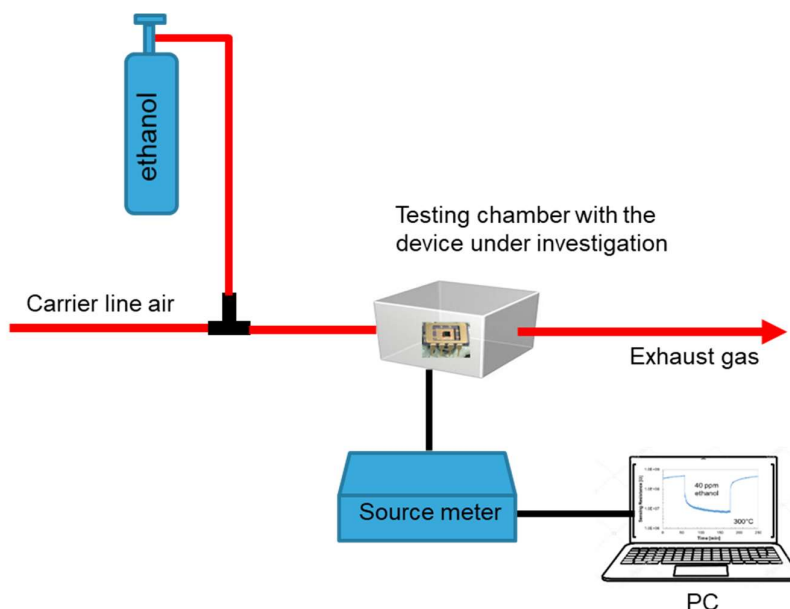**Figure 7.** Gas sensing measuring system.

The R_{air} progressively increased at 190 °C and 230 °C likely due to a structural modification of the deposited film (increasing of the baseline). When the ethanol gas was introduced inside the chamber, the resistivity of the sensing layer increased, with a response time of about 10 s (step-up in the resistivity), and decreased with a comparable response time of about 10 s when the ethanol gas flow was switched off (step back of the resistivity). After the ethanol flow was switched off, the resistivity value did not get back to the initial value. We argue that, during the test, the temperature promoted a rearrangement of the initial crystal lattice towards the formation of the anatase phase, as seen by our structural results. In this respect, a stabilization process must be framed into the production steps of the sensor for production.
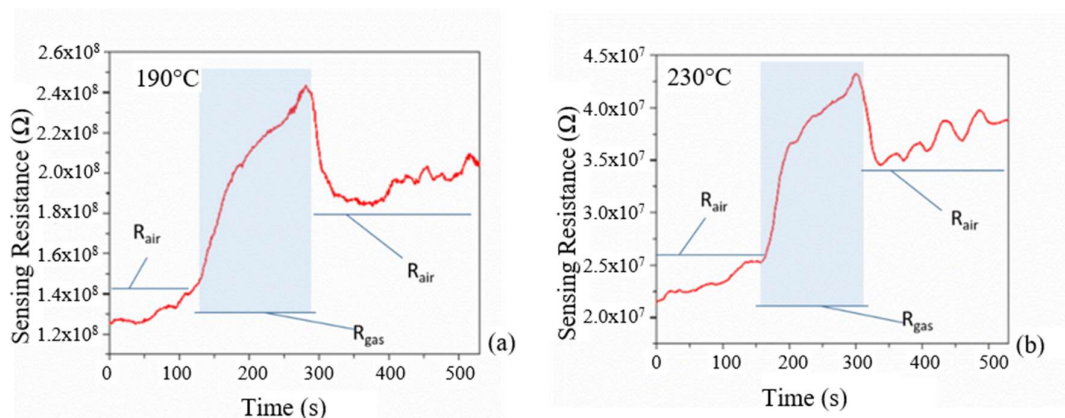

Figure 8. Sensor response to 44 ppm (concentration value after calibration) of ethanol at different working temperatures of (**a**) 190 °C and (**b**) 230 °C in the dry condition.

A drastic change of the sensor response was obtained keeping the device at a working temperature of 350 °C for 240 min. As shown by XPS analyses, the nitrogen atoms were initially located in a substitutional position inside the film. This created a level inside the band gap above the valence band of the pure TiO_2 giving the p-type character [21]. The annealing reset this doping condition in short laps of time as demonstrated by XPS analyses. An intermediate case was found by annealing at 350 °C since 240 min were needed to complete nitrogen release and to observe the change in the sensor behavior from p-type to n-type.

After this in situ annealing, the sensor turned to an n-type response, characterized by a decrease in the resistance of the material according to the well-established surface-depletion model (Figure 9). The evaluation on the responsivity, figured by the formula: $(R_{air} - R_{gas})/R_{air} \times 100$, after injection of 44 ppm of ethanol in a dry condition and working temperature of 350 °C, provided a sensing response of $51.4 \pm 0.1\%$. The sensor detection limit was 10 ppm. We chose to explore the gas sensor capability of the material in a concentration range that provided a clear response, remaining low enough for potential applications in the detection of main hazardous volatile species. The experiment allowed for the definition of a process window for a working response of the N-doped gig-lox TiO_2 sponge in the range 200–350 °C.
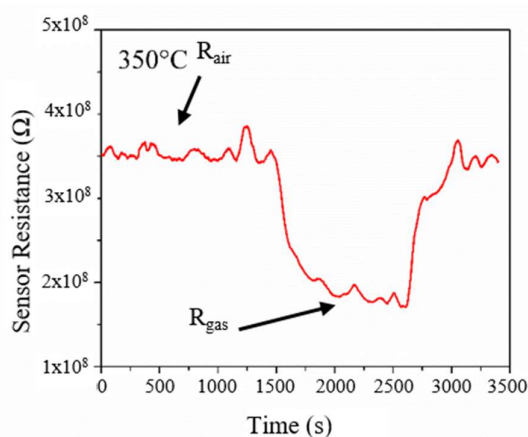
Figure 9. Sensor response to 44 ppm of ethanol when a constant value of R_{air} was achieved at 350 °C.

5. Conclusions

P-type nitrogen doping through modified gig-lox methodologies is feasible even at room temperature. The doping procedure does not penalize the multibranched nature of gig-lox oxides. Doping was performed at room temperature and was maintained up to 350 °C during ex-situ annealing. Further raising of the temperature was inconvenient for the doping as well as for the porosity preservation.

As a drawback, nitrogen introduced as reactive gas reduced the deposition rate of the TiO_2 layer mainly due to competing N–O reactions through the plasma region. The optimal doping was obtained using 2 sccm of nitrogen, although the surface-to-volume ratio was in favor of the layer deposited at 5 sccm. This is due to properly incorporated nitrogen atoms that were mainly positioned in a substitutional position with respect to the oxygen in the TiO_2 lattice at the low N_2 flow rate, giving the layer a clear p-type character. Accordingly, the sensor exhibited a p-type response to ethanol species with the resistance rising by a factor 2 at $\approx$200 °C under operation. In the range of 350–500 °C, the sensor turned to n-type as the ones made of undoped TiO_2 films. The phenomenon was related to a loss of the nitrogen content inside the film during the annealing. Low-temperature operation and a stabilizing procedure before operation are featured by our experiment that would render the sensor applicable on flexibles substrates. Sensitivity to other gas species with similar, or even superior, surface reactivity as the ethanol species is addressed and can be explored in future works.

The integration of the N-doped gig-lox TiO$_2$ sponge at room temperature on a sensing device is simple and can be done as the last production step. Thin layers are required for sensing (~400 nm), and working temperatures are low. Easy TiO$_2$ doping procedures, combined with porosity, are of general purpose and interest for several applications.

Conflicts of Interest: The authors declare no conflict of interest.

References

1. Bai, J.; Zhou, Q. Titanium Dioxide Nanomaterials for Sensor Applications. *Chem. Rev.* **2014**, *114*, 10131–10176. [CrossRef] [PubMed]

2. Dey, A. Semiconductor metal oxide gas sensors: A review. *Mater. Sci. Eng. B* **2018**, *229*, 206–217. [CrossRef]

3. Sabri, Y.M.; Kandjan, A.E.; Rashid, S.S.A.A.H.; Harrison, C.J.; Ippolito, S.J.; Bharg, S.K. Soot template TiO$_2$ fractals as a photoactive gas sensor for acetone detection. *Sens. Actuators B Chem.* **2018**, *275*, 215–222. [CrossRef]

4. Zhang, Y.; Yang, Q.; Yang, X.; Deng, Y. One-step synthesis of in-situ N-doped ordered mesoporous titania for enhanced gas sensing performance. *Microporous Mesoporous Mater.* **2018**, *270*, 75–81. [CrossRef]

5. Ceotto, M.; Lo Presti, L.; Cappelletti, G.; Meroni, D.; Spadavecchia, F.; Zecca, R.; Leoni, M.; Scardi, P.; Bianchi, C.L.; Ardizzone, S. About the Nitrogen Location in Nanocrystalline N-Doped TiO$_2$: Combined DFT and EXAFS Approach. *J. Phys. Chem. C* **2012**, *116*, 1764–1771. [CrossRef]

6. Shen, H.; Mi, L.; Xu, P.; Shen, W.; Wang, P. Visible-light photocatalysis of nitrogen-doped TiO$_2$ nanoparticulate films prepared by low-energy ion implantation. *Appl. Surf. Sci.* **2007**, *253*, 7024–7028. [CrossRef]

7. Peng, F.; Cai, L.; Yu, H.; Wang, H.; Yang, J. Synthesis and characterization of substitutional and interstitial nitrogen-doped titanium dioxides with visible light photocatalytic activity. *J. Solid State Chem.* **2008**, *181*, 130–136. [CrossRef]

8. Asahi, R.; Morikawa, T. Nitrogen complex species and its chemical nature in TiO$_2$ for visible-light sensitized photocatalysis. *Chem. Phys.* **2007**, *339*, 57–63. [CrossRef]

9. Zhao, Z.; Liu, Q. Mechanism of higher photocatalytic activity of anatase TiO$_2$ doped with nitrogen under visible-light irradiation from density functional theory calculation. *J. Phys. D Appl. Phys.* **2008**, *41*, 025105. [CrossRef]

10. Di Valentin, C.; Pacchioni, G.; Selloni, A.; Livraghi, S.; Giamello, E. Characterization of Paramagnetic Species in N-Doped TiO2 Powders by EPR Spectroscopy and DFT Calculations. *J. Phys. Chem. B* **2005**, *109*, 11414–11419. [CrossRef]

11. Sanzaro, S.; Smecca, E.; Mannino, G.; Bongiorno, C.; Pellegrino, G.; Neri, F.; Malandrino, G.; Catalano, M.R.; Condorelli, G.G.; Iacobellis, R.; et al. Multi-Scale-Porosity TiO$_2$ scaffolds grown by innovative sputtering methods for high throughput hybrid photovoltaics. *Sci. Rep.* **2016**, *6*, 39509. [CrossRef]

12. Sanzaro, S.; Fazio, E.; Neri, F.; Smecca, E.; Bongiorno, C.; Mannino, G.; Puglisi, R.A.; La Magna, A. Pervasive infiltration and multi-branch chemisorption of N-719 molecules into newly designed spongy TiO$_2$ layers deposited by gig-lox sputtering processes. *J. Mater. Chem. A* **2017**, *5*, 25529. [CrossRef]

13. Alberti, A.; Renna, L.; Sanzaro, S.; Smecca, E.; Mannino, G.; Bongiorno, C.; Galati, C.; Gervasi, L.; Santangelo, A.; La Magna, A. Innovative spongy TiO$_2$ layers for gas detection at low working temperature. *Sens. Actuators B* **2018**, *259*, 658–667. [CrossRef]

14. Alberti, A.; Bongiorno, C.; Pellegrino, G. Anatase/Rutile nucleation and growth on (0002) and (11-20) oriented ZnO:Al/glass substrates at 150 °C. *Solid Film* **2014**, *555*, 3–8. [CrossRef]

15. Pellegrino, G.; Bongiorno, C.; Ravesi, S.; Alberti, A. Fiber texturing in nano-crystalline TiO$_2$ thin films deposited at 150 °C by dc-reactive sputtering on fiber-textured [0001] ZnO:Al substrates. *J. Phys. D Appl. Phys.* **2012**, *45*, 355301. [CrossRef]

16. Asahi, R.; Morikawa, T.; Irie, H.; Ohwaki, T. Nitrogen-Doped Titanium Dioxide as Visible-Light-Sensitive Photocatalyst: Designs, Developments, and Prospects. *Chem. Rev.* **2014**, *114*, 9824–9852. [CrossRef]

17. Saha, N.C.; Tompkins, H.G. Titanium nitride oxidation chemistry: An X-ray photoelectron spectroscopy Study. *J. Appl. Phys.* **1992**, *72*, 3072–3079. [CrossRef]

18. Delegan, N.; Daghrir, R.; Drogui, P.; El Khakani, M.A. Bandgap tailoring of in-situ nitrogen-doped TiO$_2$ sputtered films intended for electrophotocatalytic applications under solar light. *J. Appl. Phys.* **2014**, *116*, 153510. [CrossRef]

19. Wu, Y.; Tseng, P.; Hsieh, P.; Chou, H.; Tai, N. High Mobility of Graphene-Based Flexible Transparent Field Effect Transistors Doped with TiO$_2$ and Nitrogen-Doped TiO$_2$. *ACS Appl. Mater. Interfaces* **2015**, *7*, 9453–9461. [CrossRef]

20. Takahashi, I. Electronic resonance and photoemission study of nitrogen doped TiO$_2$ rutile (1 1 0) single crystals. *Appl. Surf. Sci.* **2012**, *259*, 320–323. [CrossRef]

21. Pan, H.; Zhang, H.Y.; Shenoy, V.B.; Gao, H. Effects of H-, N-, and (H, N)-Doping on the Photocatalytic Activity of TiO$_2$. *J. Phys. Chem. C* **2011**, *115*, 12224–12231. [CrossRef]

22. Asahi, R.; Morikawa, T.; Ohwaki, T.; Aoki, K.; Taga, Y. Visible-Light Photocatalysis in Nitrogen-Doped Titanium Oxides. *Science* **2001**, *293*, 269–271. [CrossRef]